Membrane poration by antimicrobial peptides combining atomistic and coarse-grained descriptions

Rzepiela, Andrzej J.; Sengupta, Durba; Goga, Nicolae; Marrink, Siewert J.

Published in:
Faraday Discussions

DOI:
10.1039/b901615e

Publication date:
2010

Membrane poration by antimicrobial peptides combining atomistic and coarse-grained descriptions

Andrzej J. Rzepiela,† Durba Sengupta,† Nicolae Goga and Siewert J. Marrink*

Received 26th January 2009, Accepted 26th March 2009
First published as an Advance Article on the web 18th August 2009
DOI: 10.1039/b901615e

Antimicrobial peptides (AMPs) comprise a large family of peptides that include small cationic peptides, such as magainins, which permeabilize lipid membranes. Previous atomistic level simulations of magainin-H2 peptides show that they act by forming toroidal transmembrane pores. However, due to the atomistic level of description, these simulations were necessarily limited to small system sizes and sub-microsecond time scales. Here, we study the long-time relaxation properties of these pores by evolving the systems using a coarse-grain (CG) description. The disordered nature and the topology of the atomistic pores are maintained at the CG level. The peptides sample different orientations but at any given time, only a few peptides insert into the pore. Key states observed at the CG level are subsequently back-transformed to the atomistic level using a resolution-transformation protocol. The configurations sampled at the CG level are stable in the atomistic simulation. The effect of helicity on pore stability is investigated at the CG level and we find that partial helicity is required to form stable pores. We also show that the current CG scheme can be used to study spontaneous poration by magainin-H2 peptides. Overall, our simulations provide a multi-scale view of a fundamental biophysical membrane process involving a complex interplay between peptides and lipids.

2 Introduction

Antimicrobial peptides (AMPs) exhibit a wide range of antimicrobial and antifungal activity and have attracted significant interest as potential antibiotics.[1–3] Although the details of the many modes of action of AMPs are still unclear, a large number of AMPs function by inducing transmembrane pores that lead to cell death.[4–6] The peptides bind to phospholipid bilayers and above a threshold concentration induce local defects in the bilayer.[7–10] A well studied example of an antimicrobial peptide is magainin, found in the skin of the African clawed frog *Xenopus laevis*.[8,11] The peptide is cationic and unstructured in solution but adopts a predominantly α-helical structure when bound to lipid bilayers.[12] At peptide lipid ratios of about 1/40, magainin peptides have been suggested to permeabilize the lipid matrix, forming water-filled, nanometer-sized toroidal-shaped pores.[7,11] Poration is associated with an increase in lipid flip-flops and the translocation of peptides across the membrane.[13]

Groningen Biomolecular Sciences and Biotechnology Institute & Zernike Institute for Advanced Materials, University of Groningen, Nijenborgh 4, 9747, AG, Groningen, The Netherlands. E-mail: S.J.Marrink@rug.nl

† These authors contributed equally to this paper.

The main characteristic of a toroidal pore is that it is hydrophilic and the peptides are believed to stabilize the pore by interacting strongly with the lipid headgroups that line the pore.[4–6] However, the exact structure of the pore, in particular the arrangement of the peptides and lipid molecules is still debated. The classical model of the toroidal pore postulates a regular structure lined with lipid head-groups and peptides.[5,6] All peptides associated with the pore are thought to remain α-helical and line the pore in a transmembrane orientation. This model of the toroidal pore assumes that peptides are orientated along the membrane surface before poration and perpendicular to the membrane in the porated state. The model does not include pore-formation by peptides with low helicity or β-strand peptides. Alternative models such as the micelle-like aggregate model,[3] disordered-toroidal pore model[14] and chaotic pore model[15,16] have been proposed. These models have helped to interpret recent NMR[17] and fluorescence data[18] and are compatible with kinetic studies.[15] These models all propose a higher degree of disorder in the pore state than had been previously assumed.

Atomistic simulations of magainin had provided the first direct evidence on the disordered nature of the toroidal pore model.[14] The simulation results, though compatible with previous experimental data, pointed to only a few peptides inserting into the toroidal-shaped pore and the other peptides lining the pore edge. Similar pores were also observed in extensive simulations of melittin interaction with DPPC bilayers.[19] The term disordered toroidal pore was coined to describe such pores. In both studies, pores were observed only above a critical peptide to lipid ratio and required local aggregation of peptides. In the two sets of simulations, the peptides showed significant loss of α-helicity and pore formation does not appear to require that the peptides remain helical. However, whether the peptides remain partially unfolded or refold in the pore state can only be addressed by longer simulations. The simulations also shed light on the possible mechanisms and driving forces of pore formation. Removing the positive charges on the AMPs blocked pore formation,[19] pointing to a mechanism similar to electroporation events. The role of electrostatic interactions in AMP action has also been studied in other simulation studies,[20] for a review see ref. 21. However, a framework allowing a comprehensive study of related peptides and lipids to analyze the driving forces of this process is difficult to achieve with atomistic simulations.

Coarse-grain (CG) force-fields allow sampling larger systems at longer time scales and thereby allow faster analyses of different systems (see ref. 22). CG simulations are still in their early stages but have already been successfully applied to analyze lipid–peptide interactions. A simple solvent-free CG simulation technique was used to study interactions between amphipathic peptides and bilayers and to explore the different conditions leading to desorbed, adsorbed and inserted configurations of the peptide.[23] The action of other AMPs have been studied using force-fields based on the MARTINI force-field.[24] A study on the interaction of maculatin on large vesicles concluded that the peptides disrupt the lamellar structures but do not form water-filled channels.[25] Alamethicin, implicated to form regular barrel-stave shaped pores, has been studied in combined atomistic/CG simulations.[26] The authors used CG simulations to equilibrate the distribution of alamethicin within the membrane and then converted the coarse-grained simulation to atomistic to investigate the details of water permeation. The simulations observed quite irregular structures, contrary to the current models in the literature that postulate a highly ordered protein channel. Simulations of a synthetic peptide, LS3 have shown that it assembles in a dehydrated barrel-stave pore.[27] Spontaneous poration and water permeation has been observed in coarse-grain studies for related pore-forming molecules such as dendrimers.[28] These studies show that CG models can be used to study the interplay between peptides and lipids over larger length and time scales; however, at the same time atomistic detail is lost and it remains questionable how realistic the configurations sampled at the CG level are. To fully understand the driving forces of this process, a multi-scale approach is required.

Here, we study the pore-forming propensity of AMPs at multiple scales combining coarse-grain and atomistic simulations. We focus on a member of the magainin family of antimicrobial peptides, magainin-H2 interacting with zwitterionic phosphatidylcholine membranes. The long-time relaxation properties of AMP-pores are studied by evolving pores formed in atomistic descriptions[14,19] with a CG representation using the MARTINI model.[24,29] To test the predictions, key states observed in the CG simulations are subsequently back transformed to an atomistic description using our recently developed resolution–transformation protocol.[30] Similar approaches have been used recently by a number of other groups to study membrane–protein interactions.[26,31–34] Overall, our simulations provide a multi-scale view of a fundamental biophysical membrane process involving a complex interplay between lipids and proteins.

3 Methods

3.1 Simulation protocol and force field

The molecular dynamics simulations were performed using the GROMACS program package[35] under periodic boundary conditions. The temperature was weakly coupled (coupling time 0.1 ps) to $T = 323$ K using a Berendsen thermostat.[36] The pressure was weakly coupled (coupling time 1.0 ps, compressibility 5×10^{-5} bar^{-1}) using a semi-isotropic coupling scheme in which the lateral ($P_|$) and perpendicular (P_z) pressures are coupled independently at 1 bar,[36] corresponding to a tension-free state of the membrane.

The atomistic system was described using the GROMOS 43a2 force field[37] for the peptides and the Berger parameters from a previous study[38] for the lipids, identical to our previous work.[14,19] A group-based twin range cut-off scheme (using cut-offs of 1.0/1.4 nm and a pair-list update frequency of once per 10 steps) including a reaction field (RF) correction[39] with a dielectric correction of 78 to account for the truncation of long-range electrostatic interactions was used. We also tested an alternative model where the electrostatic interactions were treated using particle mesh ewald (PME) summation and found that the pores formed using RF were also stable with PME. The water was described using the SPC model.[40] A time step of 2 fs was used. Bond lengths were constrained using the LINCS algorithm.[41]

The MARTINI force-field[24,29] was used to describe the coarse-grain system. The force-field is based on a four-to-one mapping, *i.e.* on average four non-hydrogen atoms are represented by a single interaction center. The force-field has been parametrized based on the reproduction of partitioning free energies between polar and apolar phases and allows an accurate representation of the chemical nature of the underlying atomistic structure. In this force-field, the backbone parameters (backbone bonded terms) are dependent on the secondary structure of the beads but independent of the amino acid. Four different systems with varying helicity—100%, 65%, 40% and 0% were modelled. Secondary structure was imposed by including a dihedral potential between backbone atoms. The force constant used in the system with 100% and 40% helicity was the standard MARTINI parameter of 400 kJ mol^{-1}. The force constant used in the system with 65% helicity was reduced to 70 kJ mol^{-1}. The value was chosen to allow greater conformational flexibility as dictated by our previous results from atomistic simulation.[14,19] In line with the decreased helicity, the polarity of the backbone bead was increased to a P5-particle, similar to the polarity of the fully-coiled system. The back-bone bead (in the helical stretch) of the fully-helical and 40%-helical peptides was of type N0. The LJ (Lennard-Jones) interactions were treated with a switch function from 0.9 to 1.2 nm (pair-list update frequency of once per 10 steps) and PME was used to treat long-range electrostatics. The use of PME is non-standard in the MARTINI force-field since it was parametrized using a shifted potential. However, in simulations of membrane poration events by dendrimers, it has been shown that the use of a PME scheme[28] is required.

Test simulations performed for our systems also indicated that membrane pores are more stable and similar to the pores observed with atomistic models when long range electrostatic interactions are taken into account. Importantly, we found that the use of PME does not significantly affect the equilibrium properties of pure lipid bilayers, including the area per lipid. In all CG simulations, a time step of 30 fs was used. The simulation times reported in the remainder of this manuscript are effective times obtained by the multiplication of the actual simulation time by a factor of four based on the speed-up achieved for diffusion of water and lipids.[24,29]

3.2 Resolution–transformation

Two types of transformation were used, either increasing or decreasing the resolution. The latter case is more trivial; here the CG lipids and peptides were mapped from the atomistic structure using the center of mass to define the CG bead positions. CG water beads were reintroduced to the system afterwards and the system was equilibrated. The case of introducing atomistic detail into a CG system is more demanding. Here we used a resolution–transformation protocol which was recently developed in our group.[30] In this three step method, the goal is to equilibrate an atomistic ensemble within the constraints imposed by the CG configuration, with the additional requirements that (i) the generated atomistic configurations represent an equilibrium ensemble, and (ii) the method is general *i.e.* can be applied to any (bio)molecular system. In short, the method proceeds along the following three steps. First, the initial positions of the atomistic particles were constructed by random insertion in a sphere of radius 0.3 nm centered at their corresponding CG beads. The mapping of the CG bead to the atomistic representation is in accordance with the MARTINI force-field. Four atomistic water molecules are mapped to a single CG bead with additional restraining potentials to keep the four water molecules grouped together. Second, a restrained simulated annealing MD procedure was employed and the temperature was gradually decreased in 40 000 steps from its starting value of 1300 K to the desired target temperature of 323 K. This allowed the system to rapidly cross energy barriers and find a low-energy minimum at the target temperature. To avoid numerical instability caused by the highly strained starting structure, force capping was applied during the simulated annealing, with forces exceeding a maximum value of 15 000 kJ mol^{-1} nm^{-1} reduced to the maximum value. Finally, the CG restraints were gradually removed in 1000 steps to ensure a smooth relaxation of the system in the full atomistic force-field. This method has been tested on various biomolecules such as lipids, cholesterol, amino-acids, short peptides and water. Details of the resolution–transformation protocol together with its verification will be published elsewhere.[30]

3.3 System set-up

Two different set-ups studying the interaction of magainin-H2 (IIKKFLHSIW KFGKAFVGEI MNI) peptides with a phosphatidylcholine lipid bilayer were simulated. The first set focused on the properties of the pore at a multi-scale level in which the resolution of the atomistic and CG structures was exchanged using the above described protocol. The starting atomistic simulations containing 4 magainin-H2 peptides and 128 DPPC lipid molecules were taken from ref. 14. The CG representation of the porated state was then mapped from the atomistic system. We mapped the 50-atom DPPC molecule to a 10-bead CG representation with 3 beads in each tail. Note that the standard MARTINI model maps DPPC to four bead tails. The precise mapping is somewhat arbitrary, however. We found that the thickness of the bilayer with three tail beads is more similar to the atomistic representation of the DPPC bilayer at the relatively high hydration level used in the atomistic studies. The second set of simulations studied poration propensity of the peptides in a CG representation. To study poration after association within the bilayer, 4 magainin-H2 peptides were placed in a transmembrane orientation inside a pre-equilibrated

bilayer containing 122 lipids. To study spontaneous pore formation mimicking a biological system, 14 peptides were placed in the aqueous phase close to a bilayer consisting of 304 lipids. Two lipid types were tested—the three tail-bead lipid as described above and a two tail-bead lipid molecule, representing a short-tail lipid. Multiple simulations were performed for each system, starting from different initial random velocity distributions.

4 Results and discussion

4.1 Comparing the atomistic and coarse-grain pores

To explore the possibilities of the CG model to study pores formed by AMPs, CG representations of the starting atomistic pore configuration were obtained and evolved with the MARTINI force-field. We focus on the pores formed by four magainin-H2 peptides in a 128 lipid DPPC bilayer. Snapshots of the starting atomistic structure (taken from the simulations reported in ref. 14), the mapped CG system, and the system evolved for 24 μs are shown in Fig 1 A, B and C. During the CG simulations, a water channel was maintained through the membrane in contrast to previous CG studies on the action of AMPs.[25–27] The topology of the porated state, in particular its disordered nature was also preserved. In the CG representation, lipid molecules and a few peptides continued to line the water channel. The remaining peptides associated with the membrane at the mouth of the pore and did not insert into the pore. The size of the pore, however, was somewhat reduced at the CG level compared to the original atomistic simulation. Toward the end of the CG simulation, after 24 μs, we increased the resolution of the system back to the atomistic level. During the subsequent 50 ns simulation at the atomistic level, the pore remained similar to the transformed atomistic structure (snapshots shown in Fig 1D, E).

In general, comparing the atomistic to CG pore structure, a number of important points become apparent from our multi-scale approach. The first is that the MARTINI model predicts a similar type of pore as seen by the atomistic model, *i.e.* a fully hydrated, toroidally shaped, pore lined by lipids and peptides. Second, as expected, the two models are not fully compatible; quantitative differences exist, evidenced for instance by the size of the pore. The third point which becomes apparent is the limited sampling which can be obtained with the atomistic model. Based on our inverse transformation from the CG level back to the atomistic level we find that the configuration sampled in the CG model, being different from the starting atomistic structure, is also stable at the atomistic level. It suggests that these configurations are either meta-stable states requiring much longer relaxation times or are equilibrium states not sampled in previous atomistic simulations. On the accessible nanosecond time scale the peptide/lipid complex is almost frozen, pointing to the importance of a multi-scale approach.

4.2 Characteristics of the CG pore

At the longer time scales probed in this multi-scale study, the disordered toroidal pore maintained its structure and topology. The main feature of the disordered toroidal pore, a term coined from our atomistic simulations,[14,19] is the presence of some surface-aligned peptides as opposed to only transmembrane orientations. We observe that the peptides did not all insert into the pore and continued to line the mouth of the pore stabilizing the membrane curvature. This pore structure varies considerably from the classical model of a toroidal pore in which the peptides all align along the membrane normal inside the pore and maintain their helicity. Our multi-scale simulations reconfirm that the disordered nature of the pore may be a more realistic model than the classical toroidal pore.

The extended simulation time reached with the CG model allows for a more quantitative analysis of the structure of the pore. Fig. 2 shows the density profile of water

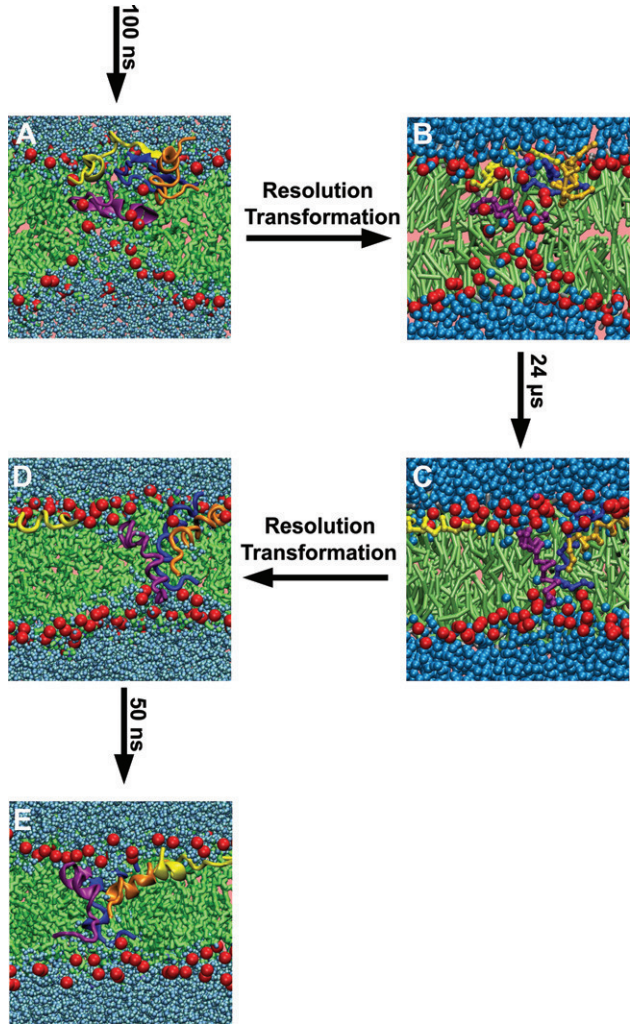

Fig. 1 The structure of the toroidal pore formed by magainin-H2 peptides in DPPC bilayers at multiple scales. A: The toroidal pore in an atomistic representation. B: A snapshot of the CG representation mapped from A. C: The CG pore after evolving the system from B for 24 μs. D: Snapshot of the atomistic representation mapped from C by using the resolution transformation protocol. E: The toroidal pore after evolving with atomistic resolution for 50 ns. All figures are prepared using VMD.[46]

and the phosphate bead of the lipid during the simulation in the porated state, compared to a pure bilayer. From the inset, it is clearly seen that water is present within the membrane in the porated state. The toroidal pores formed in the CG study are therefore hydrated, and a water flux through the pore was observed. Though a water channel is maintained through the bilayer, the flux through the pore is not constant. Large fluctuations were also seen in the position of the lipid head-groups. At a given time, only a few lipid molecules inserted into the pore. The lipid molecules flip flop through the pore from one leaflet to another as observed in other simulations.[42–44] Twelve flip-flop events were counted over the 30 μs trajectory. At the microsecond time scale, the peptides sampled different orientations and transitions between the transmembrane and surface aligned states are observed

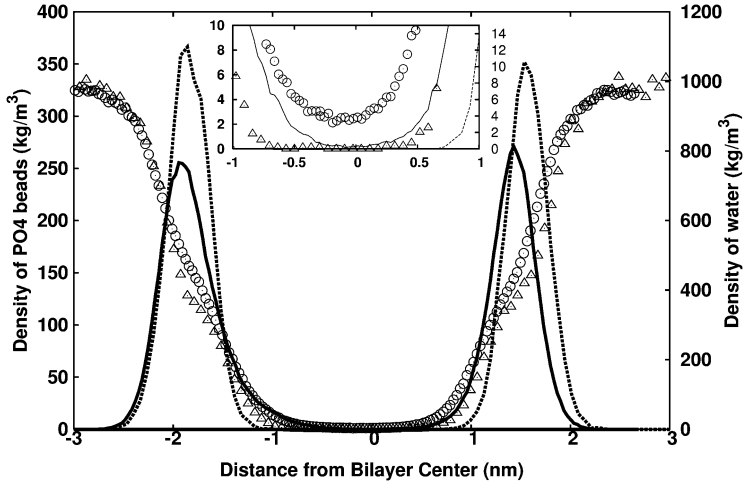

Fig. 2 The density of water and the phosphate bead of the lipids in CG simulations of a pure DPPC bilayer (△ and - - - respectively) and in a porated membrane with 4 magainin-H2 peptides (○ and —, respectively). The inset clearly shows the higher water density in the bilayer in the presence of the peptides.

(Fig. 3). It is seen that one out of the four peptide remains surface-bound on the same leaflet. Another peptide translocates through the pore from an inserted state to the other leaflet. The remaining two peptides insert into the pore from a surface-aligned orientation. Although significant peptide movement is observed, especially compared to motions probed in the atomistic simulations, it appears that a microsecond time scale is still not sufficient to sample equilibrium orientations of the peptides.

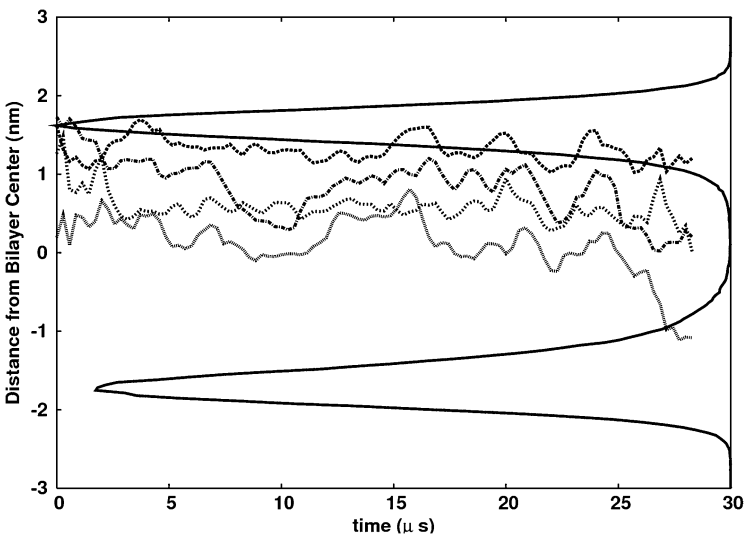

Fig. 3 The center of mass of the four peptides (dashed and dotted lines) in a toroidal pore evolved with a CG representation. The bold line shows the density profile of the phosphate beads of the lipid head-groups during the simulation.

4.3 Effect of helicity on pore stability

In the CG peptide model, secondary structure is imposed on the peptides and the choice of defining the helicity in the peptides was somewhat arbitrary. In the atomistic simulations, widely differing helicity was observed ranging between 30% and 70%. In the first scenario we imposed 65% helicity on all peptides which is slightly higher than the average helicity observed in the atomistic simulations. The pore was stable in this case and the pore state was maintained as described above. Increasing the helicity to full helicity, decreased the stability of the pore. Fewer lipid molecules inserted into the pore and the water flux also decreased substantially. In four independent simulations (starting from different random velocities), the pore closed on a microsecond time scale. Similarly, decreasing helicity completely (fully coil state) or to 40% decreased the stability of the pore, although the pore remained open in these cases. Fig. 4 shows the density of water inside the pores, for different peptide helicity. The water contained within the pore was the highest for the first peptide model (65% helicity) and decreased in the other peptide models. Thus, partial helicity is required for stabilizing pores formed by magainin-H2 peptides in membranes. This is in line with experimental data showing that increasing helicity in synthetic peptides decreased antimicrobial activity.[45] Note that even for the fully unstructured peptides, amphipathicity is maintained and they bind to the membrane. The release of secondary structure allows the peptides to sample a broader range of conformations. This is reflected by the radius of gyration, R_g shown in Fig. 5. The radius of gyration for the fully helical peptide is the largest, with lowest fluctuations, and that of the fully coiled and 40% helical peptides are the lowest with the largest fluctuations. The peptides with 65% helicity have a radius of gyration and fluctuations intermediate to the two. Note that the dihedral potentials applied in this scenario were lower than the standard MARTINI potential applied to the fully helical and 40% helical peptides. It appears that this level of flexibility of the peptide is ideal *i.e.* it can span the membrane in an extended configuration and at the same time favorably interact with the curved membrane, stabilizing a porated state. The current simulations provide evidence that an optimum helicity is required for membrane poration by AMPs.

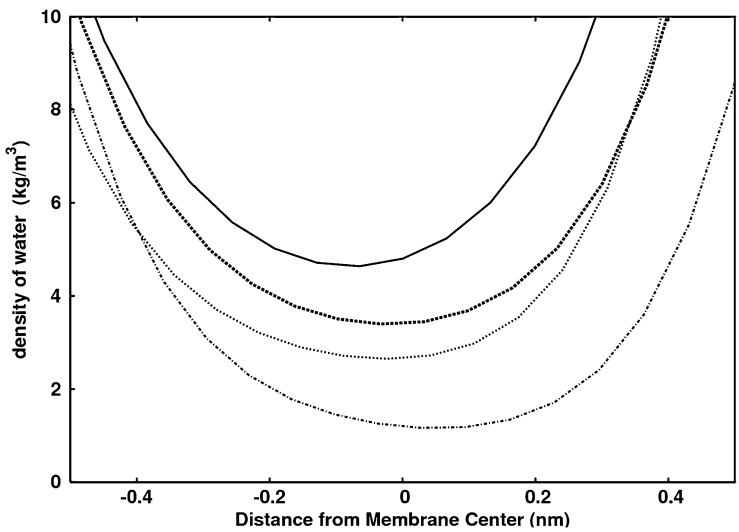

Fig. 4 The density profile of the water beads in the center of the bilayer in the CG simulations at varying peptide helicity: fully helical (dot-dashed), 65% helicity (solid line), 40% helicity (dotted) and fully flexible (dashed). The calculations for the fully helical peptide were performed on the trajectory before the pore closed. The data was fitted with a Bezier curve.

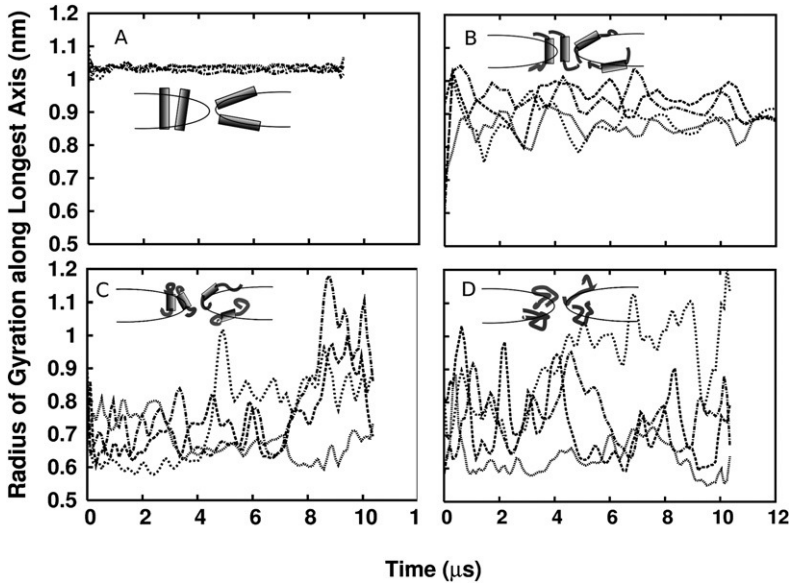

Fig. 5 Radius of gyration, R_g of the four peptides in CG simulations with peptide helicity A: 100% B: 65% C: 40% and D: 0%.

4.4 Spontaneous pore formation in CG models

The CG models in the previous sections were biased towards the starting atomistic structures and we carried out further tests to determine the equilibrium structures predicted by the CG model. Two sets of simulations were performed, either with the peptides pre-inserted into the membrane or with the peptides initially placed randomly in the aqueous phase. In the first set-up, four magainin-H2 peptides, constrained at 65% helicity, were inserted into the membrane in a transmembrane orientation as shown in Fig. 6A. The peptides were observed to diffuse laterally in the membrane to assemble into aggregates of three or more peptides, in four independent simulations. A snapshot of the simulation at the beginning of the aggregation is shown in Fig. 6B. The peptide aggregates perturbed the lamellar state considerably and large fluctuations in the lipid head-group positions were seen. The peptides

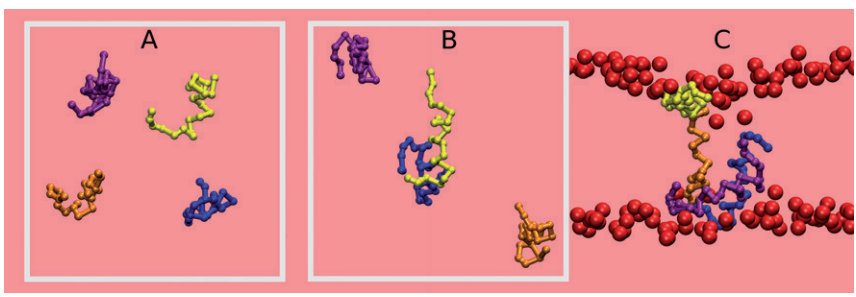

Fig. 6 The time course of events when four magainin-H2 peptides are inserted into a DPPC bilayer modeled at the CG level. A: Top view of the starting structure. Note that the peptides are inserted in a transmembrane orientation. B: Top view of the system after 20 ns. C: Snapshot of the toroidal pore after 5 μs. The phosphate beads of the lipids are shown in red and the four peptides in purple, yellow, orange and blue. The tails of the lipid molecules and the water is not shown for clarity.

along with the fluctuations in the bilayer eventually initiated a water channel and opened a pore (Fig. 6C). In the pore, a few peptides lined the pore and the remaining peptides were surface-aligned. Clear transitions were seen between the transmembrane and surface aligned orientations. The structure of the pore is essentially the same as obtained from the resolution transformation (section 4.1). We also tested cases with peptides constrained at 0%, 40% and 100% helicity. The fully helical structures assembled in the bilayer and opened a water channel with very low water density in the membrane core, reminiscent of the dehydrated barrel-stave pore observed in the simulations of synthetic peptides.[27] No lipid head-groups were inserted into the core of the membrane and lipid flip flop did not occur. The peptides with 40% helicity and fully coiled peptides induced a fluctuating toroidal-shaped water channel through the membrane. However, the flux through the membrane was lower than in the case of the 65% helical peptides. Partial helicity appears to be a criterion to initiate and stabilize pore formation in the coarse-grain model, in agreement with our results for the resolution transformation simulation (section 4.3).

In the second set-up, simulations were performed with the peptides initially placed in water close to one leaflet of the bilayer. This setup is similar to the atomistic simulations and mimics the actual biological process of spontaneous pore formation by the AMPs. The set-up comprised 304 lipids and 14 magainin-H2 peptides (modeled with 65% helicity). The peptides remained membrane bound at the 4 μs simulation period and did not insert into the membrane. Large fluctuations were seen in the head-groups of the lipids but no pore formation occurred. It appears that the barrier associated with opening of a water channel is relatively high in the CG model preventing pore formation even at the high P/L ratio. Therefore, a two tail-bead lipid model was also tested representative of a short tail lipid. The time course of the

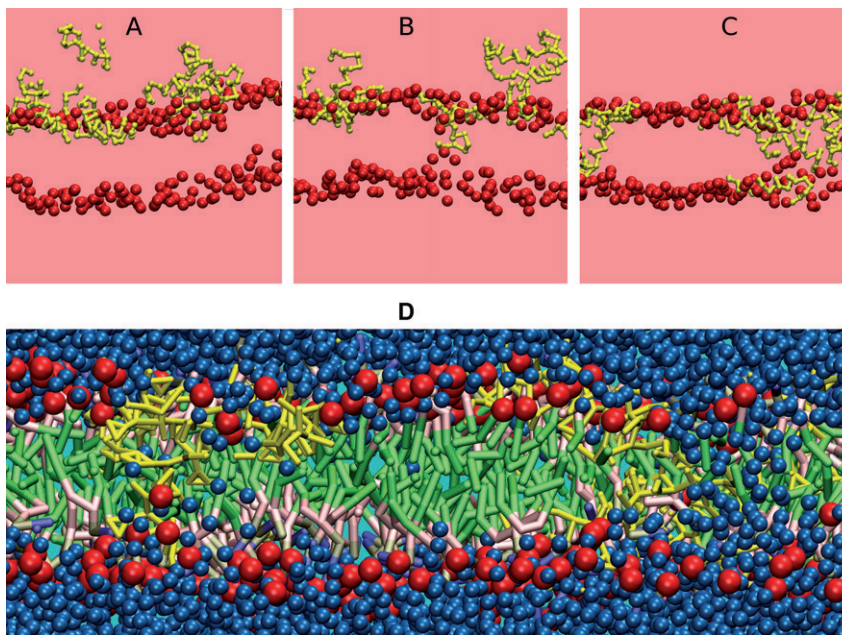

Fig. 7 The time course of events when fourteen magainin-H2 peptides are placed initially in water close to the surface of a short tail PC bilayer. A: Side view of the starting structure, B: The system after 200 ns, C: The toroidal pore after 3 μs. The phosphate beads of the lipids are shown in red and the peptides in yellow. The tails of the lipid molecules and the water are not shown for clarity. D: The toroidal pore in C shown in more detail. The lipid chains are shown in green and the water in blue.

simulation is depicted in Fig 7. The peptides adsorbed at the surface of the membrane within 10 ns. The peptides associated only after adsorption to the membrane surface. After association, they once again induced fluctuations in the head-groups of the lipid molecules and in contrast to the thicker three tail-bead membrane, spontaneous opening of a water pore was observed. In fact two pores were formed, a larger one containing nine peptides and a smaller one with five peptides (see Fig 7D). The structure of the pores was similar to the pores described above. The pores remained stable over the 3 μs simulation. Note that a pure two tail-bead CG bilayer is stable, so the poration is caused by the peptides. The results in this section point out that, even with a CG description, one may easily end up in meta-stable states and sampling remains incomplete on the microsecond time scale.

5 Conclusions

The work presented here is one of the first examples of using a multi-scale simulation framework to study membrane poration by antimicrobial peptides. Using a CG model we are able to approach time-scales compatible with experimental studies of pore formation, whereas a model with atomistic resolution provides a useful check to the accuracy of the CG model. We find that the pore structure obtained with the CG model is similar to the disordered pore seen in atomistic simulations. The pore retains its disordered character and lipid flip flop as well as water permeation through the pore is observed. At a microsecond time scale, peptides translocate *via* the pore to the other bilayer leaflet and both surface aligned and transmembrane orientations are seen in the porated state. Subsequent back-transformation of the newly generated CG structures reveal their stability also at the atomistic level of resolution. From our multi-scale simulations it appears that the disordered nature of the pore is a more realistic model than the classical toroidal pore. However, there remain some problematic sampling issues. Even the microsecond range probed by the CG model is not sufficient to sample the possible peptide orientations inside the pore. Despite these limitations, the CG model opens the way to explore the structure/activity relationship in a systematic way. Here we tested the effect of different peptide helicities on pore stability. We conclude that partial helicity is required to form and stabilize pores. Spontaneous poration events can also be studied at a CG level. Starting from a well separated, transmembrane orientation the peptides associate and induce disordered toroidal pores. A few peptides translocate to either leaflet pointing towards the importance of surface aligned peptides in stabilizing membrane curvature. Mimicking the biological situation, we simulated the attack of magainin-H2 peptides from water. Poration in this case is observed only when the energy barrier is lowered by decreasing the thickness of the bilayer. The high energy barriers to spontaneous pore formation in the CG model is presumably due to the lack of explicit electrostatic screening and polarization effects in the current MARTINI water model. Nevertheless, the sequence of events leading to pore formation, as well as the structure and size of the pore are similar to those observed in atomistic studies. The current work on the action of magainin-H2 peptides on membranes provides a multi-scale view of a fundamental biophysical membrane process involving a complex interplay between peptides and lipids.

6 Acknowledgment

This work was supported by the Netherlands Organization for Scientific Research (NWO) through their TOP and ALW Open programs. Computational access to the supercomputers of the Netherlands National Computing Facilities (NCF) is also acknowledged. The help of Martti Louhivuori in providing access to this facility is greatly appreciated.

References

1 K. L. Brown and R. E. Hancock, *Curr. Opin. Immunol.*, 2006, **18**, 24–30.
2 M. Zasloff, *Nature*, 2002, **415**, 389–395.
3 R. E. W. Hancock and D. S. Chapple, *Antimicrob. Agents Chemother.*, 1999, **43**, 1317–1323.
4 B. Bechinger and K. Lohner, *Biochim. Biophys. Acta*, 2006, **1758**, 1529–1539.
5 Y. Shai, *Biopolymers*, 2002, **66**, 236–248.
6 K. A. Brogden, *Nat. Rev. Microbiol.*, 2005, **3**, 238–250.
7 K. Matsuzaki, S. Yoneyama and K. Miyajima, *Biophys. J.*, 1997, **73**, 831–838.
8 H. Huang, *Biochim. Biophys. Acta*, 2006.
9 A. S. Ladokhin, M. E. Selsted and S. H. White, *Biophys. J.*, 1997, **72**, 1762–1766.
10 C. E. Dempsey, *Biochim. Biophys. Acta*, 1990, **1031**, 143–161.
11 K. Matsuzaki, K. Sugishita, N. Ishibe, M. Ueha, S. Nakata, K. Miyajima and R. M. Epand, *Biochemistry*, 1998, **37**, 11856–11863.
12 B. Bechinger, *J. Membr. Biol.*, 1997, **156**, 197–211.
13 K. Matsuzaki, O. Murase, N. Fujii and K. Miyajima, *Biochemistry*, 1996, **35**, 11361–11368.
14 H. Leontiadou, A. E. Mark and S. J. Marrink, *J. Am. Chem. Soc.*, 2006, **128**, 12156–12161.
15 S. M. Gregory, A. Cavenaugh, V. Journigan, A. Pokorny and P. F. F. Almeida, *Biophys. J.*, 2008, **94**, 1667–1680.
16 P. H. Axelsen, *Biophys. J.*, 2008, **94**, 1549–1550.
17 A. J. Mason, A. Marquette and B. Bechinger, *Biophys. J.*, 2007, **93**, 4289–4299.
18 L. E. Yandek, A. Pokorny, A. Floren, K. Knoelke, U. Langel and P. F. F. Almeida, *Biophys. J.*, 2007, **92**, 2434–2444.
19 D. Sengupta, H. Leontiadou, A. E. Mark and S. J. Marrink, *Biochim. Biophys. Acta, Biomembr.*, 2008, **1778**, 2308–2317.
20 F. Jean-Francois, J. Elezgaray, P. Berson, P. Vacher and E. J. Dufourc, *Biophys. J.*, 2008, **95**(12), 5748–5756.
21 E. Matyus, C. Kandt and D. P. Tieleman, *Curr. Med. Chem.*, 2008, **14**(12), 2789–2798.
22 *Coarse-Graining of Condensed Phase and Biomolecular Systems*, ed. G. A. Voth, CRC-Press, Boca Raton, 2008.
23 G. Illya and M. Deserno, *Biophys. J.*, 2008, **95**, 4163–4173.
24 L. Monticelli, S. K. Kandasamy, X. Periole, R. G. Larson, D. P. Tieleman and S. J. Marrink, *J. Chem. Theory Comput.*, 2008, **4**, 819–834.
25 P. J. Bond, D. L. Parton, J. F. Clark and M. S. P. Sansom, *Biophys. J.*, 2008, **95**(8), 3802–3815.
26 L. Thogersen, B. Schiott, T. Vosegaard, N. C. Nielsen and E. Tajkhorshid, *Biophys. J.*, 2008, **95**, 4337–4347.
27 P. Gkeka and L. Sarkisov, *J. Phys. Chem. B*, 2009, **113**, 6–8.
28 H. Lee and R. G. Larson, *J. Phys. Chem. B*, 2008, **112**, 7778–7784.
29 S. J. Marrink, H. J. Risselada, S. Yefimov, D. P. Tieleman and A. H. de Vries, *J. Phys. Chem. B*, 2007, **111**, 7812–7824.
30 A. J. Rzepiela, L. V. Schäfer, N. Goga, H. J. Risselada, A. H. de Vries and S. J. Marrink, *J. Comp. Chem.*, 2009, in press.
31 T. Carpenter, P. J. Bond, S. Khalid and M. S. P. Sansom, *Biophys. J.*, 2008, **95**, 3790–3801.
32 A. Y. Shih, P. L. Freddolino, S. G. Sligar and K. Schulten, *Nano Lett.*, 2007, **7**, 1692–1696.
33 P. Liu, Q. Shi, E. Lyman and G. A. Voth, *J. Chem. Phys.*, 2008, **129**, 114103–1141038.
34 A. Villa, C. Peter and N. F. A. van der Vegt, *Phys. Chem. Chem. Phys.*, 2009, **11**, 2077–2086.
35 D. van der Spoel, E. Lindahl, B. Hess, G. Groenhof, A. E. Mark and H. J. C. Berendsen, *J. Comput. Chem.*, 2005, **26**, 1701–1718.
36 H. J. C. Berendsen, J. P. M. Postma, W. F. van Gunsteren, A. D. Nola and J. R. Haak, *J. Chem. Phys.*, 1984, **81**, 3684–3690.
37 W. F. van Gunsteren, X. Daura, and A. E. Mark, *Encyclopedia of Computational Chemistry*, vol. 2, John Wiley and Sons, New York, 1998.
38 C. Anézo, A. H. de Vries, H. D. Höltje, D. P. Tieleman and S. J. Marrink, *J. Phys. Chem. B*, 2003, **107**, 9424–9433.
39 G. Tironi, R. Sperb, P. E. Smith and W. F. van Gunsteren, *J. Chem. Phys.*, 1995, **102**, 5451–5459.
40 H. J. C. Berendsen, J. P. M. Postma, W. F. van Gunsteren, and J. Hermans, *Interaction models for Water in Relation to Protein Hydration*, Reidel, Dordrecht, 1981.
41 B. Hess, H. Bekker, H. J. C. Berendsen and J. G. M. Fraaije, *J. Comput. Chem.*, 1997, **18**, 1463–1472.
42 D. P. Tieleman and S. J. Marrink, *J. Am. Chem. Soc.*, 2006, **128**, 12462–12467.
43 A. A. Gurtovenko and I. Vattulainen, *J. Phys. Chem. B*, 2007, **111**, 13554–13559.
44 S. J. Marrink, A. H. De Vries and D. P. Tieleman, *Biochim. Biophys. Acta, Biomembr.*, 2009, **1788**, 149–168.

45 Y. Chen, C. T. Mant, S. W. Farmer, R. E. W. Hancock, M. L. Vasil and R. S. Hodges, *J. Biol. Chem.*, 2005, **280**, 12316–12329.
46 W. Humphrey, A. Dalke and K. Schulten, *J. Mol. Graphics*, 1996, **14**, 33–38.